Vertical Coupling between Waveguides and Optical Fibers Utilizing Polarization Gratings

Xiangyu Xue, Enes Lievens, Brecht Berteloot, Yu-Tung Hsiao, Lukas Van Iseghem, Gilles Freddy Feutmba, Wim Bogaerts, Kristiaan Neyts, Jeroen Beeckman

***Abstract*—We present how a conventional Si waveguide grating coupler can be integrated with a polymerizable liquid crystal polarization grating to provide vertical coupling between optical fibers and planar waveguides. The implementation involves the deposition of a liquid crystal polymer film onto the surface of the planarized photonic chip. To achieve optimal performance, both the period and thickness of the thin film grating are optimized through a two-dimensional finite element simulation. The simulation results indicate that the output beam can be entirely redirected towards the vertical direction. We demonstrate a fabricated device and experimental validation of the proposed device in a laboratory setting. Through the verification, we affirm the feasibility of the proposed concept.**

***Index Terms*—Grating coupler, high-contrast waveguides, vertical coupling, polarization grating, liquid crystal polymer.**

I. Introduction

EFFICIENTLY coupling light to and from optical fibers is a challenge for silicon photonics due to modal size differences. This is tackled using in-plane (edge) and off-plane (vertical) coupling methods. In edge coupling, a fiber is aligned horizontally with an on-chip waveguide at the chip facet, providing high coupling efficiency, wide bandwidth, and low polarization-dependent loss. However, this approach demands precise facet polishing and limits flexibility, adding fabrication cost and reducing alignment tolerance. Vertical grating couplers offer flexibility in coupling positions, but with lower coupling efficiency compared to edge couplers. Numerous researches are dedicated to enhancing coupling efficiency [1–4].

Traditional grating couplers use angled fibers to achieve high coupling efficiencies and to prevent second-order reflection, but the need for angled fibers encumbers wafer-scale tests and economical packaging. Having a grating coupler that emits light in a perfectly vertical manner would reduce complexity in surface-emitting and receiving devices. This can notably decrease packaging expenses and simplify the process by aligning with vertical emission. Various techniques have been proposed to achieve this perfectly vertical emission [5–8]. In these methods asymmetry is introduced into the grating to enhance coupling efficiency in the vertical direction. Other options are using non-uniform periodic grating couplers [9–11], the implementing double-layer grating couplers [12, 13] or making 2D variation of grating couplers [14] with the goal of achieving vertical coupling. These approaches demand the application of high-resolution deep ultraviolet (DUV) etch. Furthermore, the attainment of low coupling loss necessitates materials that are not CMOS compatible, such as the inclusion of a Au reflective layer inside the SOI stack [11].

The liquid crystal polarization grating (LCPG) is widely recognized for its high efficiency in diffracting light beams, exceeding 99% diffraction into the +1 order [15–17]. Due to its ability to gradually manipulate the phase of a beam, the LCPG avoids abrupt changes in light phase, making it theoretically capable of achieving 100% diffraction efficiency. The efficiency of the LCPG relies on its thickness (d), while the diffraction angle is determined by its period (Λ). The creation of a continuously rotating optical axis for the LCPG is facilitated by the photoalignment method, which can be achieved through the interference of two laser beams or by utilizing a spatial light modulator (SLM) [16, 18, 19].

In this work we propose to address the fiber to chip coupling issue by applying a LCPG on top of the grating couplers of a photonic chip. It is crucial that the light propagating within the waveguide remains linearly polarized, as polarization gratings work with circularly polarized light. To achieve this, an additional quarter waveplate (QWP) needs to be placed underneath the LCPG. Ideally, both the QWP and LCPG can be created by spin-coating polymerizable liquid crystal onto photo-alignment patterns that have been prepared in advance. The thickness of the LC device can be adjusted by altering the concentration of the LC mixture or through multi-layer spin-coating techniques [20, 21].

II. FEM simulation

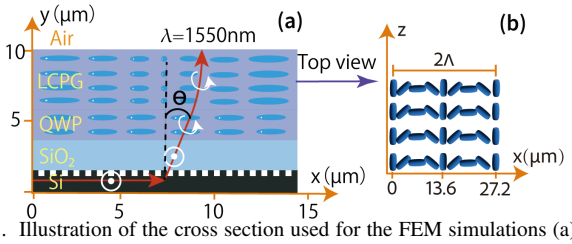

Fig. 1. Illustration of the cross section used for the FEM simulations (a). Top view of the orientation of the LC in the LCPG (b).

Simulations are conducted using COMSOL to demonstrate the feasibility of this concept. Utilizing the Finite Element

Xiangyu Xue, Enes Lievens, Brecht Berteloot, Yu-Tung Hsiao, Gilles Freddy Feutmba, Kristiaan Neyts, Jeroen Beeckman are with the Liquid Crystal and Photonics Research Group, ELIS Department, Ghent University, 9052 Ghent, Belgium (e-mail: Xiangyu.Xue@UGent.be; Enes.Lievens@UGent.be; Brecht.Berteloot@UGent.be; Yu-Tung.Hsiao@UGent.be; GillesFreddy.Feutmba@UGent.be; Kristiaan.Neyts@UGent.be; Jeroen.Beeckman@UGent.be).

Enes Lievens, Gilles Freddy Feutmba, Lukas Van Iseghem, Wim Bogaerts are with the Photonics Research Group, Department of Information Technology, Ghent University-imec, 9052 Ghent, Belgium. (e-mail of Lukas Van Iseghem and Wim Bogaerts: Lukas.Vaniseghem@UGent.be; Wim.Bogaerts@ugent.be)

Method (FEM) [22], light propagation from a single mode Si waveguide coupled to air using a grating coupler is simulated. The schematic representation of the simulated structure, shown in Figure 1(a) illustrates the two-dimensional simulation configuration, from bottom to top: Si waveguide and grating coupler, SiO_2, a quarter wave plate (QWP), a liquid crystal polymer grating (LCPG), and air. The parameters for the grating coupler are taken from the IMEC ISiPP50G platform with a Si thickness of 220 nm and an etch depth of 70 nm. The grating period is 630 nm for an operation wavelength of 1550 nm. The TE mode is coupled out into the SiO_2 layer and undergoes conversion into circularly polarized light through the QWP, subsequently experiencing a deflection to the vertical orientation (θ = 0°) by the LCPG. The top view shows the rotating optical axis of the LCPG, as depicted in Figure 1(b). A complete rotation of the optical axis, spanning 360°, is referred to as 2Λ. Since the grating couplers emit light around a 12° angle in air, we employ the well-known diffraction equation to match the LCPG period with that angle: $\sin\theta_{out} = (m\frac{\lambda}{\Lambda}) + \sin\theta_{in}$ (with $m = 1$), yielding $\Lambda = 13.6$ μm. For optimal efficiency of the LCPG, achieving a thickness of a half-wave plate (HWP) is essential. This thickness, calculated through $\Gamma = \frac{2\pi}{\lambda}(n_e - n_o)d = \frac{\pi}{2}$, equates to $d = 4.3$ μm. Here, Γ stands for the retardation, while $n_e = 1.687$ and $n_o = 1.508$ represent the extraordinary and ordinary refractive indices, respectively.

Here, we present simulation results for three distinct cases: the bare grating coupler planarized with SiO_2 (a), the same including the LCPG layer (b), and the arrangement incorporating both the QWP and LCPG (c). The resultant electric field plots for these structures are presented in Figure 2(a), (b), and (c), correspondingly. On the simulation area's boundary,

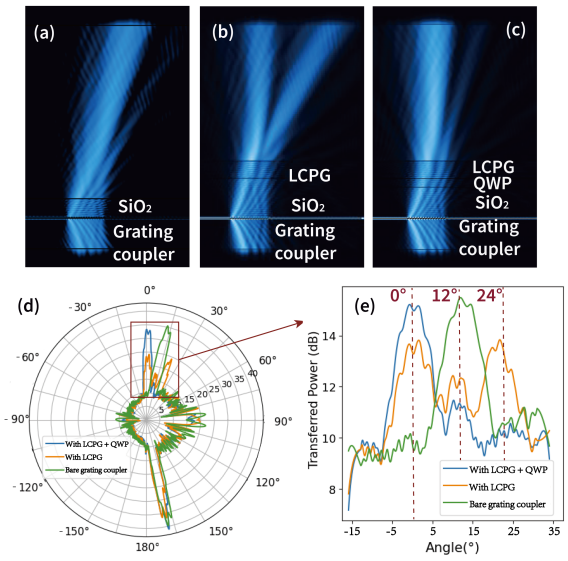

Fig. 2. Simulated electric field plots for three scenarios: (a), (b), and (c). The far-field representation depicting the radiation pattern is shown in (d). A closer examination within the range of -15° to 35° is magnified in (e).

the far field can be computed, as illustrated in Figure 2(d). It shows the light extracted from the bare grating coupler undergoes an approximate 12° deviation from the vertical direction. Upon integration of the LCPG, the light beam is effectively divided into two directions: one perpendicular and the other doubled in angle. Notably, when the QWP and LCPG layers are combined, the light goes only to the perpendicular direction. Upon closer examination in Figure 2(e), a little decline in efficiency is discernible from model (a) to model (c). Furthermore, model (b) shows two peaks, each exhibiting a roughly 3 dB drop compared to model (a), equating to a halving of power for each peak.

III. Fabrication

In the illustrated manufacturing procedure (as shown in Figure 3), we chose a waveguide made through an Imec Multi-Project Wafer run for Si photonic passive chips. This waveguide is accompanied on both of its sides by a pair of grating couplers. The following step is to apply a photoalignment layer (SD-1) onto the chip through spin-coating.

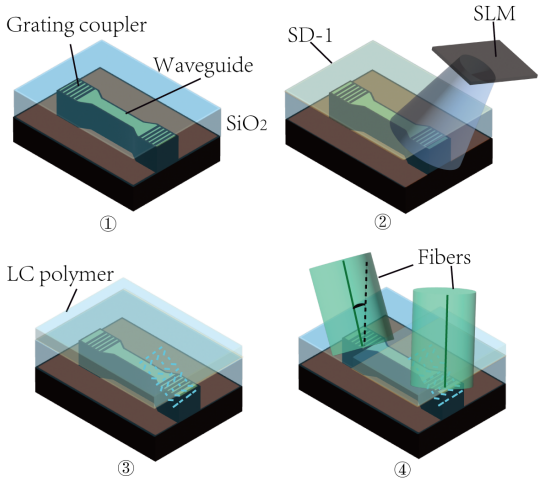

Fig. 3. Illustration of the manufacturing process for LCPG.

Subsequently, the chip is illuminated using a setup with a SLM to create a grating pattern with a period of 13.6μm [23]. The composition of the LC mixture and the multilayer spin-coating process can be found in references [20, 21].

Spin-coating multiple layers of LC on top of each other is a commonly used technique, for example to achieve multi-twist retarders [24]. In our fabricated devices, no QWP has been integrated, only a LCPG. This is because the photoalignment material used in this work cannot be spincoated onto a polymerized LC layer because the solvent attacks the previously deposited polymer. Recently developed photoalignment materials that can be dissolved in water or other less aggressive solvents have been reported [25, 26] that can enable multi-layer devices with different alignment.

The last procedure involves eliminating the LC polymer from unwanted locations. This can be achieved by employing adhesive tape over the regions where the LC polymer requires removal. Once the tape is firmly applied to the film, it is left in position for 5 minutes. Following this, the tape is meticulously peeled off, resulting in the complete removal of the LC polymer thin film from the silicon chip. As a result, we obtain a sample where only one of the two grating couplers at the sides of the straight waveguide, which will be measured using fibers, is covered by the LCPG.

IV. Characterization

Initially, the samples are subjected to microscopic examination for characterization. On the left side of the grating

coupler, the polymer layers were deliberately removed. As depicted in Figure 4(a), the grating coupler is devoid of any residual material. Conversely, on the right side of the gratings,

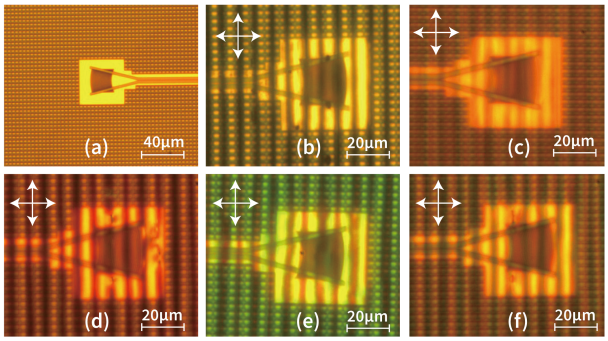

Fig. 4. Reflective optical microscope images of the grating couplers. The LC polymer in (a) is peeled off. Grating couplers in (b)-(f) are covered with 1, 3, 5, 7 and 9 spin-coated layers of LCPG, respectively.

the coupler is covered by the LCPG layer, which is illustrated in Figure 4(b)-(f). In polarizing microscopy, alignment of the LC optical axis with either the polarizer or the analyzer results in a dark appearance within the image; conversely, a non-parallel orientation produces brightness. The peak brightness is observed for an azimuthal angle of 45°. These gratings exhibit distinct bright and dark lines when viewed between crossed polarizers, with a periodicity of 6.8 μm (conforming to the definition of polarization gratings, wherein 2 bright and 2 dark lines constitute one period of 13.6 μm), aligning with the expectations. The variations in color are attributed to the closely matched thicknesses of these LC layers with those of half-wave plates of different colors. The small bright dots observed on the chip are dummy tiling patterns in regions without photonic structures.

The thickness of the LC polymer layers was measured using a profilometer. A clear linear relationship between the number of layers and the corresponding thickness was observed, as illustrated in Figure 5.

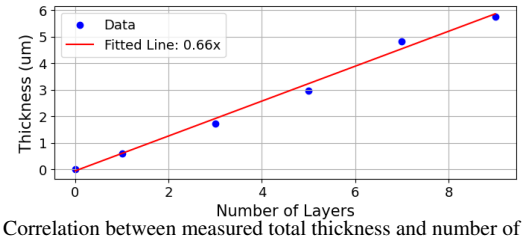

Fig. 5. Correlation between measured total thickness and number of deposited LC polymer layers.

Figure 6 depicts the experimental arrangement for the fiber-to-chip measurement. The input fiber remains fixed at an angle of 12°, while the output fiber is adjustable within the range of 0° to 24°. With each adjustment in angle, a repositioning step is necessary to determine the optimal out coupling power.

To assess the influence of LCPGs, we conduct data analysis by subtracting the transmitted power of samples containing LCPGs from the power transfer of unaltered samples. This enables us to quantify the precise power variation attributable to the presence of LCPGs. Figure 7(a) to (c) illustrate the subtracted power values for samples with thicknesses of 2.97 μm, 4.82 μm, and 5.76 μm, respectively. In general, the curves at 0° and 22° exhibit higher power levels, while the curves at 10°, 12°, and 14° show minimum power levels, consistent

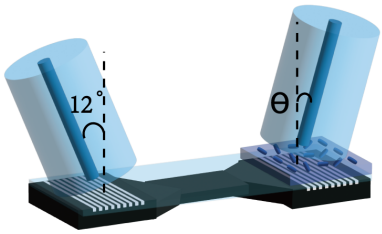

Fig. 6. Setup for fiber-to-chip measurement. The angle of the fiber at the left side is fixed at 12°, while the angle θ of the fiber at the right-hand side can be changed from 0° to 24°.

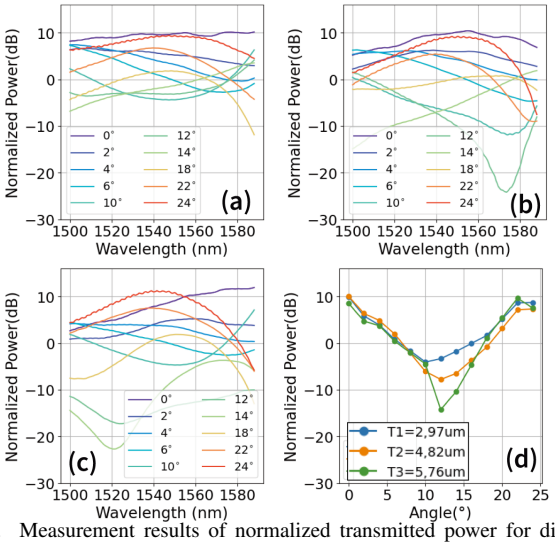

Fig. 7. Measurement results of normalized transmitted power for different number of LC layers (3, 5, and 7) as shown in (a), (b), and (c) respectively. Transmitted power for 1550 nm for layer count (3, 5, and 7) (d).

with the simulation results. In Figure 7(b), a dip is observed in the 12° curve at 1570 nm, while in Figure 7(c), the dip is shifted to 1525 nm. This indicates that as the layer thickness increases, the dip experiences a blue shift. Similarly, a peak in the 24° curve at 1550nm in Figure 7(b) is shifted to 1540 nm in Figure 7(c). Moreover, the 24° curve shows a ripple, which can be attributed to a Fabry-Perot effect.

Additionally, Figure 7 (d) depicts the values of power changes plotted against the fiber probe tilt angles for the three samples, measured at 1550 nm. The plot illustrates that the power transfer at 0° and 24° is comparable and forms two peaks at around 10dB, while the curves collectively dip at approximately 12°. This indicates that the light beam, initially emitted at 12°, has now been redirected to 0° and 24°. This aligns precisely with the expected results from our simulation.

The power transfer levels at 0° and 24° is relatively consistent, whereas at 12°, the power decreases from -3dB to -15dB with an increase in the layer thickness. The ideal thickness differs from what was predicted in the simulations, potentially due to an overestimation of Δn in the LCPG. As a result, in practice, a thicker polymer layer might be necessary to provide adequate compensation.

To compare the coupling efficiency, Figure 8 depicts four lines: two dashed lines for simulations and two for measured data. Red lines show simulated and measured 12° coupling without LCPG, and blue lines represent simulated and measured 0° coupling with optimized LCPG. Simulated data indicates a 3dB difference at 1550nm, matching expectations. Experimental data shows a 4.2dB variance, revealing an addi-

tional 1.2dB loss with actual LCPG. In experiments, the 12° coupling line has a 1dB loss band over 17nm, while the 0° coupling with LCPG has a 1dB loss band spanning 32nm.

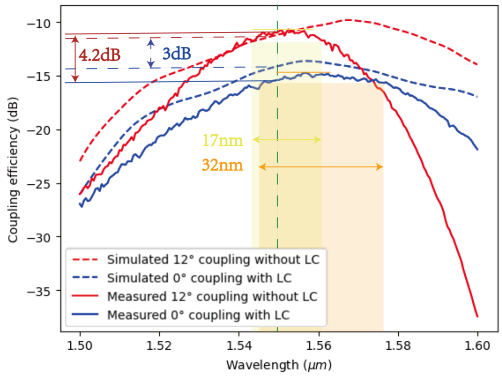

Fig. 8. Comparison of coupling efficiency between simulation and experimental data at 0° and 12° angles.

The polymer shows prolonged durability and remarkable resilience. Our longest-preserved sample remains unchanged for over a year. The cost-effective fabrication method contrasts traditional photonics chip production, offering an affordable and feasible option for post-processing of photonic chips.

V. Conclusion

In this work, an LCPG is applied on top of a grating coupler of a planarized Si photonic chip. The LCPGs are fabricated through a multi-step process involving spin-coating of a reactive mesogen (RM) mixture, followed by solvent evaporation and photopolymerization. It is demonstrated that such a LCPG can be used to transform standard Si photonic grating couplers into vertical light coupling devices which can greatly simplify photonic packaging. We demonstrate the application of the LCPGs on the IMEC ISiPP50G, but the techique can be easily adapted to other nanophotonic platforms. Both the thickness and the period of the LCPG can be adjusted in the fabrication process to accomodate for different wavelengths and/or coupling angles. Due to the planarization of the photonic chip with 2 μm of oxide the light propagation in the waveguides is unafected by the LCPG, but it is demonstrated that a simple peel-off procedure can be used to remove the polymer layer from regions where it is unwanted.

In this work only an LCPG without a QWP beneath was fabricated. Further work is planned with more complex LCPG designs and devices in which LC layers with different alignment are combined to demonstrate advanced beam shaping of light exiting the grating couplers.

References

[1] Y. A. Vlasov and S. J. McNab, "Losses in single-mode silicon-on-insulator strip waveguides and bends," *Optics express*, vol. 12, no. 8, pp. 1622–1631, 2004.

[2] T. Alder, A. Stohr, R. Heinzelmann, and D. Jager, "High-efficiency fiber-to-chip coupling using low-loss tapered single-mode fiber," *IEEE Photonics Technology Letters*, vol. 12, no. 8, pp. 1016–1018, 2000.

[3] N. Hattasan, B. Kuyken, F. Leo, E. M. Ryckeboer, D. Vermeulen, and G. Roelkens, "High-efficiency soi fiber-to-chip grating couplers and low-loss waveguides for the short-wave infrared," *IEEE Photonics Technology Letters*, vol. 24, no. 17, pp. 1536–1538, 2012.

[4] L. Cheng, S. Mao, Z. Li, Y. Han, and H. Y. Fu, "Grating couplers on silicon photonics: Design principles, emerging trends and practical issues," *Micromachines*, vol. 11, no. 7, 2020. [Online]. Available: https://www.mdpi.com/2072-666X/11/7/666

[5] B. Wang, J. Jiang, and G. P. Nordin, "Embedded slanted grating for vertical coupling between fibers and silicon-on-insulator planar waveguides," *IEEE Photonics Technology Letters*, vol. 17, no. 9, pp. 1884–1886, 2005.

[6] J. Schrauwen, S. Scheerlinck, D. Van Thourhout, and R. Baets, "Polymer wedge for perfectly vertical light coupling to silicon," in *Integrated Optics: Devices, Materials, and Technologies XIII*, vol. 7218. SPIE, 2009, pp. 99–106.

[7] D. Benedikovic, C. Alonso-Ramos, D. Pérez-Galacho, S. Guerber, V. Vakarin, G. Marcaud, X. Le Roux, E. Cassan, D. Marris-Morini, P. Cheben *et al.*, "L-shaped fiber-chip grating couplers with high directionality and low reflectivity fabricated with deep-uv lithography," *Optics Letters*, vol. 42, no. 17, pp. 3439–3442, 2017.

[8] A. Michaels and E. Yablonovitch, "Inverse design of near unity efficiency perfectly vertical grating couplers," *Optics express*, vol. 26, no. 4, pp. 4766–4779, 2018.

[9] S. Hooten, T. Van Vaerenbergh, P. Sun, S. Mathai, Z. Huang, and R. G. Beausoleil, "Adjoint optimization of efficient cmos-compatible si-sin vertical grating couplers for dwdm applications," *Journal of Lightwave Technology*, vol. 38, no. 13, pp. 3422–3430, 2020.

[10] T. Watanabe, M. Ayata, U. Koch, Y. Fedoryshyn, and J. Leuthold, "Perpendicular grating coupler based on a blazed antiback-reflection structure," *Journal of Lightwave Technology*, vol. 35, no. 21, pp. 4663–4669, 2017.

[11] J. Liu, Z. Zheng, B. Chen, Z. Wang, C. Li, K. Chen, and L. Liu, "High-performance grating coupler array on silicon for a perfectly-vertically mounted multicore fiber," *Journal of Lightwave Technology*, vol. 40, no. 16, pp. 5654–5659, 2022.

[12] M. Dai, L. Ma, Y. Xu, M. Lu, X. Liu, and Y. Chen, "Highly efficient and perfectly vertical chip-to-fiber dual-layer grating coupler," *Optics Express*, vol. 23, no. 2, pp. 1691–1698, 2015.

[13] T. Van Vaerenbergh, S. Hooten, M. Jain, P. Sun, Q. Wilmart, A. Seyedi, Z. Huang, M. Fiorentino, and R. Beausoleil, "Wafer-level testing of inverse-designed and adjoint-inspired dual layer si-sin vertical grating couplers," *Journal of Physics: Photonics*, vol. 4, no. 4, p. 044001, 2022.

[14] Y. Tong, W. Zhou, and H. K. Tsang, "Efficient perfectly vertical grating coupler for multi-core fibers fabricated with 193 nm duv lithography," *Optics Letters*, vol. 43, no. 23, pp. 5709–5712, 2018.

[15] J. Kim, Y. Li, M. N. Miskiewicz, C. Oh, M. W. Kudenov, and M. J. Escuti, "Fabrication of ideal geometric-phase holograms with arbitrary wavefronts," *Optica*, vol. 2, no. 11, pp. 958–964, 2015.

[16] T. Zhan, J. Xiong, Y.-H. Lee, R. Chen, and S.-T. Wu, "Fabrication of pancharatnam-berry phase optical elements with highly stable polarization holography," *Optics express*, vol. 27, no. 3, pp. 2632–2642, 2019.

[17] B. Gao, J. Beeckman, and K. Neyts, "Design and realization of a compact efficient beam combiner, based on liquid crystal pancharatnam–berry phase gratings," *Crystals*, vol. 11, no. 2, p. 220, 2021.

[18] V. G. Chigrinov, V. M. Kozenkov, and H.-S. Kwok, *Photoalignment of liquid crystalline materials: physics and applications*. John Wiley & Sons, 2008.

[19] B. Berteloot, I. Nys, X. Xue, J. Beeckman, and K. Neyts, "Rotationally invariant ring-shaped liquid crystal structures between two substrates with different photoalignment," *Journal of Molecular Liquids*, vol. 337, p. 116238, 2021.

[20] X. Xue, B. Berteloot, M. Stebryte, K. Neyts, and J. Beeckman, "Role of homeotropic alignment strength at the air interface of polymerized liquid crystal layers," *Optical Materials Express*, vol. 11, no. 12, pp. 4036–4050, 2021.

[21] X. Xue, I. Nys, K. Neyts, and J. Beeckman, "Influence of period and surface anchoring strength in liquid crystal optical axis gratings," *Soft Matter*, vol. 18, no. 16, pp. 3249–3256, 2022.

[22] K.-J. Bathe, "Finite element method," *Wiley encyclopedia of computer science and engineering*, pp. 1–12, 2007.

[23] I. Nys, B. Berteloot, and G. Poy, "Surface stabilized topological solitons in nematic liquid crystals," *Crystals*, vol. 10, no. 9, p. 840, 2020.

[24] R. K. Komanduri, K. F. Lawler, and M. J. Escuti, "Multi-twist retarders: broadband retardation control using self-aligning reactive liquid crystal layers," *Optics Express*, vol. 21, no. 1, pp. 404–420, 2013.

[25] R. Advincula, M.-K. Park, A. Baba, and F. Kaneko, "Photoalignment in ultrathin films of a layer-by-layer deposited water-soluble azobenzene dye," *Langmuir*, vol. 19, no. 3, pp. 654–665, 2003.

[26] A. A. Muravsky, A. A. Murauski, and A. S. Yakovleva, "47.1: Green technology of photoalignment layer coating from h2o solution for achromatic polymerizable liquid crystal retarder," in *SID Symposium Digest of Technical Papers*, vol. 54. Wiley Online Library, 2023, pp. 333–335.